Cerebral Cortex, September 2020;30: 4847–4857

doi: 10.1093/cercor/bhaa077
Advance Access Publication Date: 11 May 2020
Original Article

ORIGINAL ARTICLE

Prefrontal Multielectrode Transcranial Direct Current Stimulation Modulates Performance and Neural Activity Serving Visuospatial Processing

Yasra Arif[1,2], Rachel K. Spooner[1,2], Alex I. Wiesman[1,2], Amy L. Proskovec[2,3], Michael T. Rezich[1,2], Elizabeth Heinrichs-Graham[1,2] and Tony W. Wilson[1,2,]

[1]Department of Neurological Sciences, University of Nebraska Medical Center, Omaha, NE 68198, USA, [2]Center for Magnetoencephalography, University of Nebraska Medical Center, Omaha, NE 68198, USA and [3]Department of Psychology, University of Nebraska, Omaha, NE 68198, USA

Address correspondence to Tony W. Wilson, Center for Magnetoencephalography, University of Nebraska Medical Center, 988422 Nebraska Medical Center, Omaha, NE 68198-8422, USA. Email: twwilson@unmc.edu.

Abstract

The dorsolateral prefrontal cortex (DLPFC) is known to play a critical role in visuospatial attention and processing, but the relative contribution of the left versus right DLPFC remains poorly understood. We applied multielectrode transcranial direct-current stimulation (ME-tDCS) to the left and right DLPFC to investigate its net impact on behavioral performance and population-level neural activity. The primary hypothesis was that significant laterality effects would be observed in regard to behavior and neural oscillations. Twenty-five healthy adults underwent three visits (left, right, and sham ME-tDCS). Following stimulation, participants completed a visuospatial processing task during magnetoencephalography (MEG). Statistically significant oscillatory events were imaged, and time series were then extracted from the peak voxels of each response. Behavioral findings indicated differences in reaction time and accuracy, with left DLPFC stimulation being associated with slower responses and decreased accuracy compared to right stimulation. Left DLPFC stimulation was also associated with increases in spontaneous theta and decreases in gamma within occipital cortices relative to both right and sham stimulation, while connectivity among DLPFC and visual cortices was generally increased contralateral to stimulation. These data suggest spectrally specific modulation of spontaneous cortical activity at the network-level by ME-tDCS, with distinct outcomes based on the laterality of stimulation.

Key words: laterality effects, magnetoencephalography, neural oscillations, spontaneous activity

Introduction

Prompt attentional shifting towards and the perception of a stimulus within the visual field are a key component of many aspects of human cognitive processing, and the neural dynamics underlying such visuospatial processing includes theta, alpha, and gamma frequency modulations, most noticeably in bilateral occipital cortices. In the alpha range, desynchronization in the occipital cortices has been reported in the presence of visual input since the seminal studies of Hans Berger, and more recently, alpha synchronization has been repeatedly associated with inhibition of visual processing (Jensen and Mazaheri 2010; Handel et al. 2011; Heinrichs-Graham and Wilson 2015a; Wiesman et al. 2018a). On the other hand, gamma synchronization in occipital cortices has been linked to active visual processing of stimulus properties such as motion and feature detection (Siegel et al. 2006; Muthukumaraswamy and Singh 2013)

and selective attention (Fries et al. 2001; Tallon-Baudry et al. 2004; Vidal et al. 2006; Doesburg et al. 2007). Finally, increases in occipital theta activity have been implicated in visual stimulus sampling (Landau and Fries 2012) and more recently tied to cross-frequency coupling with the faster gamma oscillations (Lisman and Jensen 2013).

Both bottom-up and top-down regulatory processes are critical for transforming visual input into cognitive representations. Of note, the previous literature has highlighted the substantial role of the prefrontal cortex in top-down modulation of visual attention and perception (Desimone and Duncan 1995; Fox et al. 2006; Noudoost and Moore 2011; Paneri and Gregoriou 2017), with the dorsolateral prefrontal cortex (DLPFC) specifically implicated in visuospatial processing (Wilson et al. 1993). While noninvasive transcranial electric and magnetic stimulation of the DLPFC has been widely employed in the modulation of cognitive processes like working memory and decision-making (Mars and Grol 2007; Boggio et al. 2010; Andrews et al. 2011; Balconi 2013), surprisingly, the effects of transcranial direct current stimulation (tDCS) of the DLPFC on visuospatial processing remain largely unexplored. tDCS is a type of noninvasive brain stimulation and is believed to alter neuronal activity in a polarity-dependent manner via the targeted delivery of low-amplitude direct current (Coffman et al. 2014; Wiesman et al. 2018b). Briefly, the administration of current leads to a change in the underlying ionic environment, thus potentially affecting resting membrane potential and synaptic efficacy (Liebetanz et al. 2002; Nitsche et al. 2003a; Jang et al. 2009; Filmer et al. 2014; Weber et al. 2014; Hunter et al. 2015; Fertonani and Miniussi 2017). However, the net impact and mechanisms involved remain an area of active investigation. A plethora of literature has examined the effects of conventional (i.e., two-sponge electrodes) tDCS on altering cognitive processes (Fregni et al. 2005; Kuo and Nitsche 2012; Coffman et al. 2014). Far fewer studies have utilized multielectrode tDCS (ME-tDCS; sometimes called high-definition tDCS), but initial reports suggest that stimulation using this technique is more focal and that the stimulation-related effects may be longer lasting (Datta et al. 2008; Datta et al. 2009; Edwards et al. 2013; Kuo et al. 2013). Of note, tDCS is widely considered to be safe, with side effects (e.g., mild skin irritation, mild tingling sensation under electrode application site, slight fatigue, and headache) being transient and generally reported to the same extent in the sham and active conditions (Nitsche et al. 2003b; Poreisz et al. 2007; Bikson et al. 2016; Woods et al. 2016).

In the current study, we utilized ME-tDCS, an established visuospatial discrimination task, and magnetoencephalography (MEG) to investigate the effects of offline stimulation targeted to the left and right DLPFC on visuospatial processing and the underlying neural dynamics. Importantly, in earlier studies, this task has been shown to trigger strong theta, alpha, and gamma oscillatory responses in bilateral occipital cortices (Wiesman et al. 2017, 2018b, 2018c). In line with our previous findings, as well as the emerging literature showing network-level effects of transcranial electrical stimulation, we hypothesized that ME-tDCS applied to the left and right DLPFC would distinctly alter behavioral performance and neural activity in the theta, alpha, and gamma range in bilateral visual cortices, as well as connectivity with the prefrontal cortices (Keeser et al. 2011; Peña-Gómez et al. 2012; Wang et al. 2014; Heinrichs-Graham et al. 2017b; Wilson et al. 2018; Wiesman et al. 2018b; McDermott et al. 2019).

Materials and Methods

Participants

Twenty-five healthy adults (10 females, 1 left-handed) with a mean age of 23.4 years (range: 19–32 years) were enrolled. Exclusionary criteria included any medical illness effecting CNS function (e.g., HIV/AIDS), any neurological or psychiatric disorder, history of head trauma, current substance abuse, and the MEG laboratory's standard exclusion criteria (e.g., ferromagnetic implants). Written informed consent was obtained from each participant after a thorough description of the study was provided, following the guidelines of the University of Nebraska Medical Center's Institutional Review Board, which approved the study protocol.

Multielectrode Transcranial Electrical Stimulation

A 4×1 electrode configuration (four cathodes surrounding a central anode; Soterix Medical, New York, New York) was used to deliver ME-tDCS to the left and right DLPFC, using the international 10/20 system (Jasper 1958; Klem et al. 1999). Each electrode had a diameter of 12 mm and was comprised of Ag/AgCl. Cz was determined by the intersection of the inion/nasion plane and the preauricular plane following the procedures of the international 10/20 system. The central anode was placed on F3 and F4, which correspond to the left and right DLPFC, respectively, based on the Okamoto et al. transformations of the scalp-based international 10/20 system into MNI space (Okamoto et al. 2004; Okamoto and Dan 2005). The cathodes for the F3 anode condition were AF3, F1, F5, and FC3, while those for the F4 anode were AF4, F2, F6, and FC4. To identify the focality and intensity of our ME-tDCS configurations, current density modeling was conducted with the Soterix HD Explore software and tissue conductivities from the literature (gray matter = 0.276, white matter = 0.126, CSF = 1.65, skull = 0.01, skin = 0.465, air = 1×10^{-7}, gel = 0.3, electrodes = 5.8×10^{7} (Datta et al. 2009; Huang et al. 2013, 2018).

Each participant completed three separate visits, each separated by at least 1 week (M = 10.8 days, SD = 7.2 days; Fig. 1). Stimulation conditions were pseudorandomized to include two anodal (one left DLPFC active and one right DLPFC active) and one sham (right or left DLPFC, counterbalanced across participants) ME-tDCS sessions. Participants were kept blind as to which visits encompassed active stimulations and sham.

During the active visits, participants underwent 20 min of 2.0-mA direct-current stimulation, plus a 30-s ramp-up period. During the period of stimulation, a battery of cognitive tasks was administered to each participant, which was designed to assess multiple domains of function and keep the participant mentally engaged. These tests included a visual memory task, verbal fluency test, and an attention task. All of these tasks were part of the NIH Toolbox (Hodes et al. 2013; McDonald 2014). The same protocol was followed in the sham visit, but no actual stimulation was applied outside of the ramping procedure. This approach was adopted so that the participant would not know if he/she was being stimulated during any given session. Following active/sham stimulation, participants were prepared for MEG recording and seated with their heads positioned within the MEG helmet. About 45 min elapsed from the end of the stimulation to the initiation of this MEG experiment, which places the experiment well within the time window for offline effects (Kuo et al. 2013). Briefly, this study found that the level of cortical

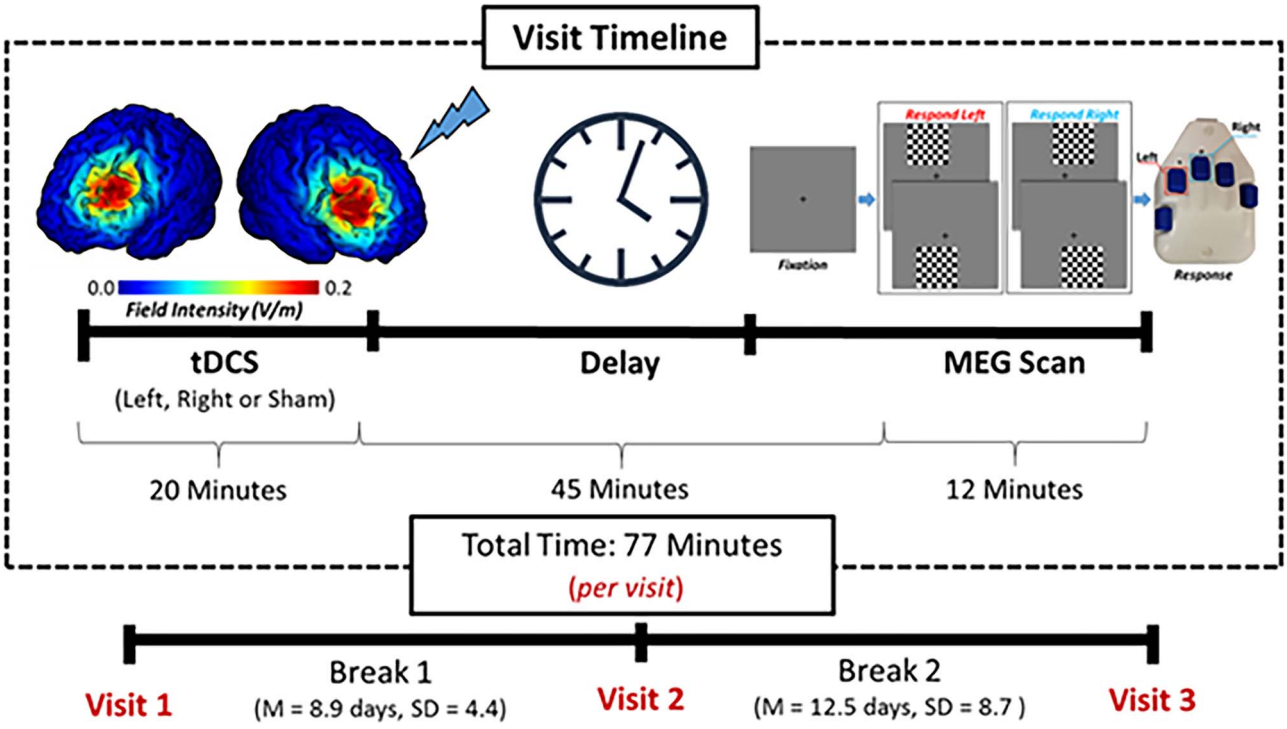

Figure 1. Experimental paradigm. Participants received 20 min of anodal and sham ME-tDCS over the left and right DLPFC. Stimulation montages were pseudorandomized across three visits, each separated by at least 1 week. Current distribution modeling revealed focused field intensity values of the left and right DLPFC (left). Following ME-tDCS participants completed a visuospatial paradigm during MEG recording (right). The total visit time from the beginning of stimulation to the end of the MEG task was approximately 77 min, which places the MEG experiment well within the peak sensitivity period for detecting offline effects of ME-tDCS (see Kuo et al. 2013). ME-tDCS, multielectrode transcranial direct current stimulation; DLPFC, dorsolateral prefrontal cortex; MEG, magnetoencephalography.

excitability peaks about 30 min after cessation of multielectrode tDCS and then slowly dissipates over the next 70–90 min. Thus, we aligned our MEG recording session to coincide with this period of neuronal excitability, which has proven effective in previous studies from our lab (Heinrichs-Graham et al. 2017b; Wilson et al. 2018; Wiesman et al. 2018b; McDermott et al. 2019).

MEG Experimental Paradigm

We used an established visuospatial discrimination task, termed *Vis-attend* (Wiesman et al. 2017, 2018b, 2018c; Wiesman and Wilson 2019). During this task, the participants were seated in a magnetically shielded room and told to fixate on a cross hair presented centrally. After a variable ISI (range: 1900–2100 ms), an 8×8 checkerboard grid was presented for 800 ms at one of four positions, relative to the fixation (i.e., one of the four visual quadrants; Fig. 1). Participants were instructed to respond via button press with their right hand whether the grid was positioned to the left (index finger) or right (middle finger) of the fixation point upon presentation of the grid. Each participant performed 240 trials (60 per checkerboard location) in a pseudorandomized order during each MEG recording.

MEG Data Acquisition

All recordings were conducted in a one-layer magnetically shielded room with active shielding engaged for environmental noise compensation. With an acquisition bandwidth of 0.1–330 Hz, neuromagnetic responses were sampled continuously at 1 kHz using an Elekta MEG system (Helsinki, Finland) with 306 sensors, including 204 planar gradiometers and 102 magnetometers. During data acquisition, participants were monitored via real-time audio–visual feeds from inside the shielded room. Each MEG dataset was individually corrected for head motion and subjected to noise reduction using the signal space separation method with a temporal extension (Taulu and Simola 2006).

Structural MRI Processing and MEG Coregistration

Prior to MEG measurement, four coils were attached to the subject's head and localized, together with the three fiducial points and scalp surface, with a 3D digitizer (FASTRAK 3SF0002, Polhemus Navigator Sciences, Colchester, VT, USA). Once the subjects were positioned for MEG recording, an electric current with a unique frequency label (e.g., 322 Hz) was fed to each of the coils. This induced a measurable magnetic field and allowed each coil to be localized in reference to the sensors throughout the recording session. As coil locations were also known with respect to head coordinates, all MEG measurements could be transformed into a common coordinate system. With this coordinate system, each participant's MEG data were coregistered with a high-resolution structural T1-weighted template brain prior to source space analysis using BESA MRI (Version 2.0). The structural MRI was in standardized Talairach space and aligned parallel to the anterior and posterior commissures. Following source analysis, each participant's $4.0 \times 4.0 \times 4.0$-mm MEG functional images were spatially resampled.

MEG Preprocessing, Time-frequency Transformation, and Sensor-Level Statistics

Eye blinks and cardio-artifacts were removed from the data using signal space projection (SSP), which was accounted for during source reconstruction (Uusitalo and Ilmoniemi 1997). The continuous magnetic time series was divided into epochs of 2700-ms duration, with 0 ms defined as the onset of the checkerboard stimulus and the baseline being the −400 to 0-ms window before stimulus onset. Epochs containing artifacts were removed based on a fixed threshold method, supplemented with visual inspection. Briefly, the amplitude and gradient distributions across all trials were determined per participant, and those trials containing the highest amplitude and/or gradient values relative to this distribution were rejected based on participant-specific thresholds (Spooner et al. 2020; Wiesman and Wilson 2020). Importantly, we used participant-specific amplitude and gradient thresholds because interindividual differences in head size, proximity to the sensors, and related variables strongly affect the amplitude of MEG signals, as magnetic field strengths decrease exponentially as the distance between the electric current source (brain) and the detector (MEG) increases. Across all conditions and participants, the average amplitude threshold was 1143.38 fT (SD = 524.22), and the average gradient threshold was 404.34 fT/epoch (SD = 142.75). On average, 214.36 (SD = 12.82) trials per participant per stimulation condition were used for further analysis, and the number of trials per participant did not significantly differ by stimulation condition, $F(2,44) = 0.869$, $P = 0.427$. The percentage of included trials per condition is as follows: left: 212.47 (88.53%), right: 214.87 (89.53%), and sham: 215.74 (89.89%).

Epochs remaining after artifact rejection were transformed into the time–frequency domain using complex demodulation (Kovach and Gander 2016) 2.0 Hz, 25 ms; range: 4–100 Hz), and the resulting spectral power estimations per sensor were averaged over trials to generate time–frequency plots of mean spectral density. These sensor-level data were normalized using the respective bin's baseline power, which was calculated as the mean power during the −400 to 0 ms-time period. This baseline period was selected to avoid possible contamination by the post-movement beta rebound (PMBR) response (Heinrichs-Graham et al. 2017a), which was confirmed by assessing this time window in the nonnormalized spectrograms. The specific time–frequency windows used for source reconstruction were determined by statistical analysis of the sensor-level spectrograms across all participants and conditions using the entire array of 204 gradiometers. Briefly, paired-sample t-tests against baseline were initially conducted on each data point, and the output spectrogram of t-values was thresholded at $P < 0.05$ to define time–frequency bins containing potentially significant oscillatory deviations across all participants and stimulation conditions. Time–frequency bins that survived the threshold were then clustered with temporally and/or spectrally neighboring bins that were also above the threshold ($P < 0.05$), and a cluster value was derived by summing the t-values of all data points in the cluster. Nonparametric permutation testing (10 000 permutations) was then used to derive a distribution of cluster values, and the significance level of the observed clusters was tested directly using this distribution (Ernst 2004; Maris and Oostenveld 2007). Further methodology details can be found in our recent papers (Spooner et al. 2019, 2020; Wiesman and Wilson 2020).

MEG Source Imaging and Statistics

Cortical networks were imaged through an extension of the linearly constrained minimum variance vector beamformer known as the dynamic imaging of coherent sources (DICS) approach (Van Veen et al. 1997; Groß et al. 2001). This beamformer calculates single images based on the cross-spectral densities of all combinations of MEG gradiometers averaged over the time–frequency range of interest and the solution of the forward problem for each location on a grid specified by input voxel space. Following convention, the source power in these images was normalized per participant using a separately averaged prestimulus noise period of equal duration and bandwidth (Hillebrand et al. 2005). Such images are typically referred to as pseudo-t maps, with units (pseudo-t) that reflect noise-normalized power differences per voxel between a baseline or passive period and an active task-based period. MEG preprocessing and imaging used Brain Electrical Source Analysis (Version 6.1; BESA) software.

Average maps across all participants were computed per condition (left active, right active, and sham) using the pseudo-t images. These average maps were used to identify the peak voxel (i.e., the voxel with the maximum amplitude value) per time–frequency response, which in all instances occurred within the left and right occipital cortices. Time series data (i.e., virtual sensors) were then extracted from these peak voxels per participant. Virtual sensors were computed by applying the sensor weighting matrix derived through the forward computation to the preprocessed signal vector, which yielded a time series for the specific coordinate in source space. Given our previous findings (Heinrichs-Graham et al. 2017b; Wilson et al. 2018; Wiesman et al. 2018b; McDermott et al. 2019), we aimed to quantify changes in both spontaneous and oscillatory neural activity per stimulation condition. Thus, we computed both relative power (i.e., relative to baseline) and absolute power time series for each peak. To examine spontaneous activity, values from the absolute power time series from each peak were averaged across the baseline period (i.e., from −400 to 0 ms). The computed values were then collapsed across hemispheres by averaging the data from the left and right occipital cortices per condition and participant. Of note, previous studies have shown that estimating local spontaneous power from such baseline periods provides very similar results to using a dedicated resting-state period (Wilson et al., 2014; Heinrichs-Graham and Wilson 2016). To examine whether ME-tDCS affected task-related oscillations, we used the relative time series data and averaged the values across the active time period used in the beamforming analyses. As with the spontaneous analysis, the computed values were averaged across hemispheres per condition and participant prior to statistical analysis. Finally, we used repeated measures 1×3 ANOVAs to identify differences between the conditions for the task-based oscillations and spontaneous activity. Any value ±3 SD from the mean was considered an outlier and removed prior to statistical analyses.

Functional Connectivity Analyses

To probe dynamic functional connectivity between the site of DLPFC stimulation and the occipital cortical regions identified in our main analyses, phase coherence was computed within the same theta, alpha, and gamma time-frequency windows derived from our sensor-level statistical analyses. Specifically, we estimated the phase locking value, PLV (Lachaux et al. 1999) between

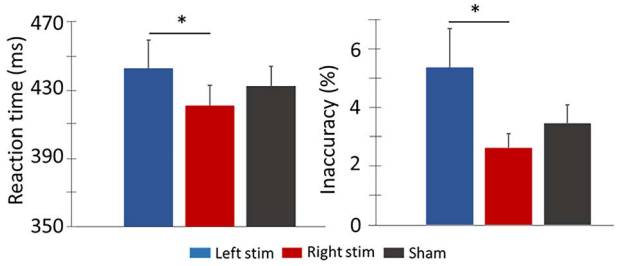

Figure 2. Behavioral performance on the visuospatial task. Stimulation montage (i.e., left and right active stimulation conditions and sham) is denoted at the bottom with the mean behavioral metrics displayed on the y-axes, with reaction to the left in ms and accuracy to the right in percentage incorrect. Following left DLPFC stimulation, participants were slower and less accurate on the task compared to performance following ME-tDCS of the right DLPFC. Error bars show the SEM. $*P < 0.05$. ME-tDCS, multielectrode transcranial direct current stimulation; DLPFC, dorsolateral prefrontal cortex; SEM, standard error of the mean.

the prefrontal sites of electrical stimulation (i.e., left and right DLPFC) and the peak voxels per time–frequency response within the left and right occipital cortices. The PLV reflects the intertrial variability of the phase relationship between pairs of brain regions as a function of time. Values close to 1 indicate strong synchronicity (i.e., phase locking) between the two brain regions within the specific time window across trials, whereas values close to 0 indicate substantial phase variation between the two signals and, thus, weak synchronicity (connectivity) between the two regions. To investigate the differential impact of stimulation montages on prefrontal–visual connectivity, we extracted the max and mean PLV per participant and condition within the time–frequency windows used for beamforming. The computed values were then averaged across occipital nodes per condition and participant, and these values were compared via 2×3 repeated measures ANOVA, with prefrontal node (left/right DLPFC) and tDCS condition (i.e., left and right anodal DLPFC and sham) as within-subject factors.

The data that support the findings of this study are available from the corresponding author, Dr Tony W. Wilson, upon reasonable request.

Results

All the participants successfully completed the study, but two were excluded due to MEG artifacts. The remaining 23 participants were 19–32 years old, with a mean age of 23.5 years.

Behavioral Effects

All participants performed in the normal range on the cognitive tests (i.e., NIH Toolbox) administered during the stimulation sessions, and there were no differences between the three stimulation conditions. In regard to the MEG task, a repeated measures 1×3 ANOVA revealed significant differences in reaction time by stimulation condition $F = 3.981$, $P = 0.031$, such that participants were slower following ME-tDCS of the left DLPFC compared to the right DLPFC (Fig. 2). A second within-subject 1×3 ANOVA probing accuracy showed that participants were also significantly less accurate, $F = 4.218$, $P = 0.038$, following ME-tDCSs of the left DLPFC compared to the right DLPFC. Thus, following active ME-tDCS of the left DLPFC, participants had longer reaction times and were less accurate (Fig. 2).

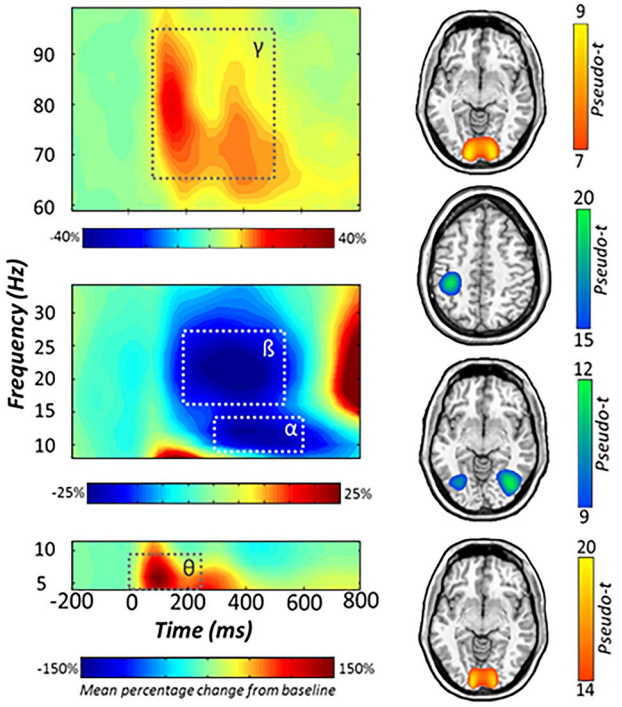

Figure 3. Neural responses to the visuospatial task. (Left): Grand-averaged time–frequency spectrograms of MEG sensors exhibiting one or more significant responses, with gamma activity at the top, alpha and beta below, and theta at the bottom. In each spectrogram, time (ms) is denoted on the x-axis and frequency (Hz) is shown on the y-axis. All signal power data are expressed as percent difference from baseline, with color legends shown below each respective spectrogram. Dashed lines indicate the time–frequency windows that were subjected to beamforming. (Right): Grand-averaged beamformer images (pseudo-t) across all participants and ME-tDCS montages for each time–frequency component. Axial slices are as follows: Gamma ($z = 1$), beta ($z = 45$), alpha ($z = -7$), and theta ($z = -9$), from top to bottom. MEG, magnetoencephalography.

Sensor-Level Analysis

Statistical analysis of the time–frequency spectrograms revealed significant clusters for four spectrally specific oscillatory responses ($P < 0.001$, corrected; Fig. 3). A large synchronization in the theta range (4–8 Hz; 0–250 ms) was observed in an array of sensors near parietal and occipital regions immediately following stimulus presentation. This response partially overlapped in time with a robust desynchronization in the beta range (18–24 Hz; 200–500 ms) and a slightly later desynchronization in the alpha band (8–14 Hz; 300–600 ms). These responses partially overlapped in space across a number of parietal and occipital sensors. Finally, a strong synchronization was observed in the gamma range (64–90 Hz; 100–500 ms), which was most prominent in MEG sensors near the occipital cortices (Fig. 3). Of note, the beta desynchronization is known to be tightly linked to motor execution (Heinrichs-Graham and Wilson 2015b, 2016; Heinrichs-Graham et al. 2016, 2017a, 2018), and thus it was imaged to confirm that its origin was the primary motor cortex (Fig. 3), but otherwise it was not further examined.

Beamformer Analysis

To localize the spatial origin of the sensor-level oscillatory responses, the aforementioned time–frequency windows of interest were imaged using a beamformer, and grand average

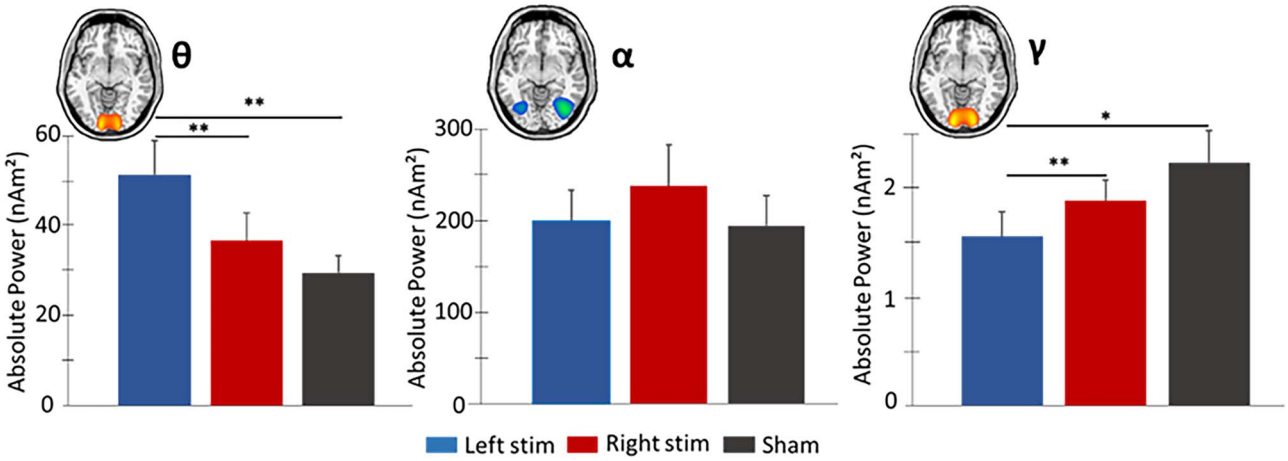

Figure 4. Spontaneous theta, alpha, and gamma activity in occipital cortices during the baseline period. Mean absolute power (nAm^2) is represented on the y-axes. Repeated measures 1×3 ANOVA were computed on spontaneous power averaged over the baseline period (−400 to 0 ms), with active conditions and sham collapsed across the hemispheres. (Left): Elevated theta power was observed following left versus right active and sham stimulation. (Middle): No significant differences were observed in spontaneous alpha power for the three conditions. (Right): Left active stimulation resulted in weaker spontaneous gamma power compared to right active and sham conditions. Error bars reflect the SEM. $*P < 0.05$. $**P < 0.01$. SEM, standard error of the mean.

maps were computed. Bilateral parieto-occipital regions showed a robust decrease in alpha power, while increases in theta and gamma power were more confined to inferior and posterior occipital cortices, bilaterally (see Fig. 3). Virtual sensors were then extracted from the peak voxels bilaterally to examine the temporal evolution of these responses for each condition. These time series were used to compute the mean absolute power spanning the baseline period, as well as the relative power during stimulus processing. In both cases, the computed values were collapsed across hemispheres per response and condition. These values were then subjected to repeated measures 1×3 ANOVA to identify the offline effects of ME-tDCS on spontaneous and task-related oscillatory activity.

A significant effect of condition was found for spontaneous theta power, $F = 9.135$, $P = 0.002$. Post hoc testing revealed that participants exhibited stronger baseline theta power following left DLPFC stimulation compared to both right DLPFC stimulation ($P = 0.004$) and sham ($P = 0.002$). In contrast, no main effect of tDCS condition was observed for baseline (basal) alpha power, $F = 2.461$, $P = 0.098$. Finally, a significant effect of condition was found for spontaneous gamma power, $F = 4.697$, $P = 0.027$. Post hoc analysis showed that participants exhibited significantly weaker baseline gamma power in occipital cortices following left compared to right stimulation of the DLPFC ($P = 0.005$) and sham ($P = 0.015$; Fig. 4).

Next, we repeated these analyses using the relative time series data to identify whether ME-tDCS affected task-related oscillatory power. Briefly, we ran three 1×3 ANOVAs (theta, alpha, and gamma), and our results indicated no significant effects for any of the three time–frequency components in occipital cortices.

Finally, we extended this approach to regions underneath the anode (F3 and F4; Okamoto et al. 2004; Okamoto and Dan 2005) and found differences in task-related alpha oscillations in the left DLPFC, $F = 4.249$, $P = 0.021$, with post hoc testing showing a significant increase in this region during left DLPFC stimulation compared to sham ($P = 0.01$). No other task-related or spontaneous differences were observed in regions underneath the anode.3.4.

Dynamic Functional Connectivity

Alterations in fronto-visual connectivity as a function of stimulation montage were evaluated using phase coherence between prefrontal sites of ME-tDCS and peak task-related activity in the bilateral occipital cortices. Briefly, we averaged the PLV between the DLPFC node (left or right) and each of the bilateral peaks (see Fig. 5) per stimulation condition and participant and then conducted a 2×3 repeated measures ANOVA per time–frequency window. We focus our results on the max PLV data, but the findings were virtually identical using the mean PLV data. For theta, there were no significant effects of stimulation condition, DLPFC node, or the interaction. In contrast, the stimulation condition by DLPFC node interaction effect was significant for alpha, $F = 3.16$, $P = 0.05$, and post hoc analyses revealed that participants exhibited stronger phase coherence between the left DLPFC and bilateral visual cortices following right stimulation relative to sham ($P = 0.025$) and marginally left stimulation ($P = 0.059$). Likewise, following left stimulation, alpha phase coherence between the right DLPFC and bilateral visual cortices was higher relative to sham ($P = 0.049$; Fig. 5). As per gamma connectivity, the stimulation by DLPFC node interaction effect was also significant, $F = 5.09$, $P = 0.01$, and post hoc analyses showed greater phase locking between the left DLPFC and bilateral visual cortices following right DLPFC stimulation relative to sham ($P = 0.012$). In addition, gamma connectivity between the right DLPFC and bilateral visual cortices was stronger following left stimulation relative to sham ($P = 0.03$) and marginally right stimulation ($P = 0.06$). Lastly, the stimulation main effect was significant for gamma ($F = 3.54$, $P = 0.04$), and follow-up tests indicated that fronto-visual connectivity was marginally stronger (both P's = 0.08) following both stimulation conditions relative to sham. No other effects were significant.

Discussion

Herein, we provide evidence for the offline neuromodulatory effects of ME-tDCS on behavioral performance (i.e., reaction time and accuracy); spontaneous (baseline) levels of theta, alpha,

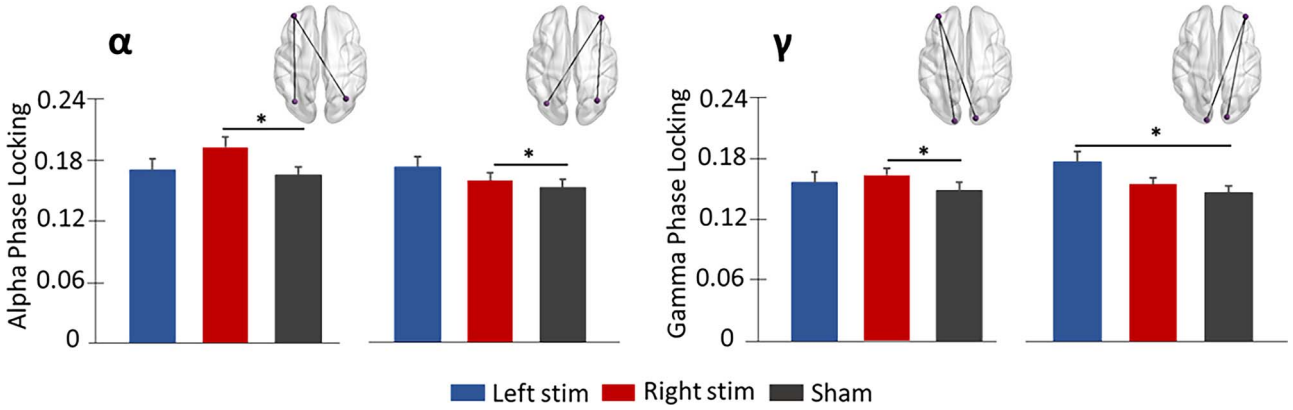

Figure 5. Differential modulation of strength of fronto-visual connectivity by stimulation montages. The glass brains represent functional connections interrogated. Phase locking value (PLV) is represented on the y-axes. Stronger alpha phase coherence was observed between left DLPFC and bilateral visual cortices versus sham following right stimulation. Left active stimulation resulted in higher phase coherence between the right DLPFC and bilateral visual cortices versus sham in alpha and gamma bands. Error bars reflect the SEM. $*P < 0.05$. SEM, standard error of the mean.

and gamma activity in the occipital region; and fronto-visual connectivity during a visuospatial discrimination task. By combining ME-tDCS with MEG and using a well-established cognitive paradigm, we were able to examine the differential behavioral and neural effects generated by left versus right DLPFC stimulation. Our results generally indicated differences in prestimulus theta and gamma power in bilateral visual cortices following targeted stimulation of the left DLPFC. We also observed differential left/right ME-tDCS effects on behavioral performance, altered alpha oscillations underneath the anode during left DLPFC stimulation, and increased alpha and gamma fronto-visual connectivity contralateral to the DLPFC being stimulated. These results and their implications are discussed in detail below.

Interestingly, behavioral performance, measured in terms of both accuracy and reaction time, significantly declined following left compared to right DLPFC stimulation. In other words, participants were less accurate in identifying the precise location of the visual stimulus and were slower in responding to the location following stimulation of the left DLPFC. Since the effect extended across both reaction time and accuracy metrics, it cannot be attributed to a speed-accuracy tradeoff and thus appears to be a broad decline in visuospatial function. Upon close inspection, the actual effect appears to be driven by participants responding slightly faster following right DLPFC stimulation compared to sham and much slower following left DLPFC compared to sham. This effect may be attributable to the right prefrontal cortex being more involved in spatial processing, whereas the left DLPFC is considered to be more involved in cognitive processes that lack a spatial component (van Asselen et al. 2006). However, this alone does not fully explain why left stimulation would negatively affect overall performance, which as stated above seemed to be the proportionally larger effect. While further work is needed, we propose that the increase in alpha and gamma functional connectivity between right DLPFC and bilateral visual cortices following left stimulation could be central to this effect. Presumably, fronto-visual connectivity in healthy adults is relatively optimized for performance, and thus increasing such connectivity could have a negative impact on behavioral performance. As discussed below, the right stimulation tended to increase alpha and gamma connectivity between the left DLPFC and bilateral visual cortices, but given the weaker role of left DLPFC in visuospatial processing, the overall impact may be more limited. Nonetheless, this framework is speculative, and additional studies are certainly needed to explore this effect in greater detail.

Occipital theta oscillations have been intimately tied to visual processing, and previous findings have signified the pivotal role of theta oscillations in the temporal organization of information transfer within the visual attention system (Fries et al. 2001; Busch et al. 2009). Herein, we found that stimulation of the left DLPFC was associated with stronger spontaneous theta activity during the baseline in bilateral occipital cortices relative to both right stimulation and sham and that left DLPFC stimulation was associated with a decline in performance. Such a pattern of results agrees with two recent studies where we linked increased spontaneous (baseline) theta activity to significantly reduced performance in a visual attention task (Lew et al. 2018; McDermott et al. 2019). In light of this literature, we propose that the modulation of baseline occipital theta following stimulation of the DLPFC likely impacted individuals' higher-order temporal decision-making processes, with the stimulation site-specific effects capturing the different roles played by the left and right DLPFC in cognitive processing (Kaller et al. 2010; Barbey et al. 2013). Of note, ME-tDCS did not strongly affect theta range functional connectivity between prefrontal and occipital cortices. Thus, the mechanism of increased spontaneous theta following left DLPFC stimulation is not entirely clear, although the concomitant changes in gamma range spontaneous activity and functional connectivity may suggest that cross-frequency coupling was involved and future studies should closely evaluate this (Lisman and Jensen 2013).

In contrast to findings in the theta range, basal gamma power in the occipital cortices was generally weaker following stimulation of the left DLPFC compared to the right and sham stimulation. Increases in gamma power, put simply, are thought to enhance the processing of visual input (Doesburg et al. 2007; Jensen and Mazaheri 2010), and it is interesting to note that the reduced occipital gamma power following left DLPFC stimulation coincided with diminished behavioral performance and increased right fronto-visual connectivity during that session. This behavioral pattern was present when utilizing

a low-level visuospatial discrimination task, and stimulation of the left DLPFC may have even greater implications for higher-order visual attention processes. Thus, the overall pattern of increased theta, decreased gamma, altered fronto-visual connectivity, and impaired behavioral performance agrees with previous literature and suggests that the stimulation of the left DLPFC had a negative impact on perceptual and neural processing. However, it should be noted that the effect of ME-tDCS on gamma (and alpha) functional connectivity was not unitary. Essentially, while left stimulation altered right fronto-visual connectivity and the right DLPFC is thought to have a larger role in spatial processing, right DLPFC stimulation was followed by increased left fronto-visual connectivity. Thus, the overall effect of ME-tDCS on functional connectivity appeared to be an increase in fronto-visual interactions involving the DLPFC that was not stimulated. Based on the behavioral data, left DLPFC stimulation was associated with prolonged reaction times and less accuracy, which could indicate that the increased gamma connectivity between the right DLPFC and bilateral visual cortices had a negative effect on spatial processing, while the increases in connectivity between the left DLPFC and bilateral visual cortices following the right stimulation had a negligible effect. However, this interpretation of the net impact of these connectivity changes is speculative, and connectivity metrics were not directly related to performance; thus, future work is needed.

Beyond the modulation of spontaneous theta and gamma activity, we observed changes in alpha range functional connectivity following ME-tDCS of the left and right DLPFC, and stimulation of the right DLPFC was also marginally linked to increased occipital alpha power during the baseline compared to left stimulation. These findings may be pertinent to future work, as a myriad of literature has shown that alterations in occipital alpha activity affect visual processing. For example, it has been shown that an elevation in occipital alpha activity leads to endogenous inhibition of visual transmission and can cause a reduction in visual discrimination efficacy if the heightened alpha stretches into the period of stimulus processing (Worden et al. 2000; Fox et al. 2006; Kelly et al. 2006; Klimesch et al. 2007; Van Dijk et al. 2008; Handel et al. 2011; Spaak et al. 2014; Wiesman et al. 2018a, 2018b). Of note, in our study, spontaneous alpha power was not predictive of task performance. Perhaps this was due to our visuospatial discrimination task being more low level (basic) in nature, whereas this pattern of modulation would have strong implications for higher-order cognitive tasks that rely on alpha-associated inhibition (e.g., working memory; see (Embury et al. 2019; Heinrichs-Graham and Wilson, 2015a, 2015b; Proskovec et al. 2016; Wilson et al. 2018). Moreover, in previous work using conventional tDCS, we found a significant elevation in occipital alpha power during the baseline using a two-sponge occipital/right prefrontal montage (Wilson et al. 2018; Wiesman et al. 2018b; McDermott et al. 2019). Thus, our finding here of a marginal increase in alpha baseline power following right DLPFC stimulation is largely consistent with this, and the reduced magnitude of the effect could be due to our use of a multielectrode montage (vs. conventional tDCS) and/or the location of stimulation in the current study. In addition, we also observed increased alpha oscillatory power in the left DLPFC following ME-tDCS of this region, although our prior findings (Wilson et al. 2018; Wiesman et al. 2018b; McDermott et al. 2019) were specific to increased spontaneous alpha during the baseline. This discrepancy could simply reflect differential effects following occipital tDCS in our prior studies versus DLPFC stimulation in the current study. Given the vast differences in cytoarchitecture between these regions (i.e., at least 2.5 times more cells per unit volume in occipital cortex relative to the DLPFC), such differential effects are not surprising. Regardless, future work in this area is needed. Finally, our alpha functional connectivity results were very similar to those observed in the gamma range. Essentially, left DLPFC stimulation was associated with increased connectivity during visuospatial processing between the right DLPFC and bilateral visual cortices relative to sham, while right DLPFC stimulation was associated with significantly increased connectivity between the left DLPFC and bilateral visual cortices relative to sham. In short, we found that connectivity was stronger between the DLPFC and bilateral visual cortices in the prefrontal node not being stimulated, which is similar to our observations in the gamma range. The impact of such alterations in connectivity on visuospatial processing is not entirely clear and should be the focus of future investigations. Further, the current findings could be extended by targeting the DLPFC with transcranial alternating current stimulation (tACS) to illuminate its effects on the neural dynamics of visuospatial attention.

In conclusion, we examined the offline neurophysiological effects of applying ME-tDCS to the left and right DLPFC, focusing on behavioral performance and neurophysiology. In agreement with previous work, we found that our visuospatial processing task elicited significant theta, alpha, and gamma oscillations in bilateral occipital cortices across all stimulation conditions (Wiesman et al. 2017, 2018b, 2018c). Importantly, we also found that spontaneous occipital theta and gamma activity during the baseline and fronto-visual alpha and gamma connectivity was altered following ME-tDCS of the DLPFC. Specifically, ME-tDCS of the left DLPFC was associated with increased occipital theta and decreased occipital gamma activity relative to sham and stimulation of the right DLPFC, whereas fronto-visual connectivity in the gamma and alpha range was generally stronger in the left DLPFC when stimulation was applied to the right DLPFC, suggesting network-level effects. Lastly, our finding of impaired task performance following ME-tDCS of the left DLPFC implies that these network effects were potentially detrimental to visuospatial function in the healthy adult brain, although it should be noted that our behavioral effects were relatively weaker than our neural effects and future studies would benefit from larger samples and greater statistical power. Such larger samples would also enable more advanced time-lag connectivity analyses, which may provide novel insight on the mechanisms of altered spontaneous activity in the visual cortices following DLPFC stimulation.

Funding

This work was supported by the National Institutes of Health (RF1-MH117032 to T.W.W., R01-MH103220 to T.W.W., R01-MH116782 to T.W.W., R01-MH118013 to T.W.W., and F31-AG055332 to A.I.W.); the National Science Foundation (#1539067 to T.W.W.).

Notes

The funders had no role in study design, data collection and analysis, decision to publish, or preparation of the manuscript.

Conflict of Interest: None declared.

References

Andrews SC, Hoy KE, Enticott PG, Daskalakis ZJ, Fitzgerald PB. 2011. Improving working memory: the effect of combining cognitive activity and anodal transcranial direct current stimulation to the left dorsolateral prefrontal cortex. *Brain Stimul*. 4:84–89.

Balconi M. 2013. Dorsolateral prefrontal cortex, working memory and episodic memory processes: insight through transcranial magnetic stimulation techniques. *Neurosci Bull*. 29: 381–389.

Barbey AK, Koenigs M, Grafman J. 2013. Dorsolateral prefrontal contributions to human working memory. *Cortex*. 49:1195–1205.

Bikson M, Grossman P, Thomas C, Zannou AL, Jiang J, Adnan T, Mourdoukoutas AP, Kronberg G, Truong D, Boggio P. 2016. Safety of transcranial direct current stimulation: evidence based update 2016. *Brain Stimul*. 9:641–661.

Boggio PS, Campanhã C, Valasek CA, Fecteau S, Pascual-Leone A, Fregni F. 2010. Modulation of decision-making in a gambling task in older adults with transcranial direct current stimulation. *Eur J Neurosci*. 31:593–597.

Busch NA, Dubois J, VanRullen R. 2009. The phase of ongoing EEG oscillations predicts visual perception. *J Neurosci*. 29:7869–7876.

Coffman BA, Clark VP, Parasuraman R. 2014. Battery powered thought: enhancement of attention, learning, and memory in healthy adults using transcranial direct current stimulation. *NeuroImage*. 85:895–908.

Datta A, Bansal V, Diaz J, Patel J, Reato D, Bikson M. 2009. Gyri-precise head model of transcranial direct current stimulation: improved spatial focality using a ring electrode versus conventional rectangular pad. *Brain Stimul*. 2:201–207 e201.

Datta A, Elwassif M, Battaglia F, Bikson M. 2008. Transcranial current stimulation focality using disc and ring electrode configurations: FEM analysis. *J Neural Eng*. 5:163.

Desimone R, Duncan J. 1995. Neural mechanisms of selective visual attention. *Annu Rev Neurosci*. 18:193–222.

Doesburg SM, Roggeveen AB, Kitajo K, Ward LM. 2007. Large-scale gamma-band phase synchronization and selective attention. *Cereb Cortex*. 18:386–396.

Edwards D, Cortes M, Datta A, Minhas P, Wassermann EM, Bikson M. 2013. Physiological and modeling evidence for focal transcranial electrical brain stimulation in humans: a basis for high-definition tDCS. *NeuroImage*. 74:266–275.

Embury CM, Wiesman AI, Proskovec AL, Mills MS, Heinrichs-Graham E, Wang Y-P, Calhoun VD, Stephen JM, Wilson TW. 2019. Neural dynamics of verbal working memory processing in children and adolescents. *NeuroImage*. 185: 191–197.

Ernst MD. 2004. Permutation methods: a basis for exact inference. *Stat Sci*. 19:676–685.

Fertonani A, Miniussi C. 2017. Transcranial electrical stimulation: what we know and do not know about mechanisms. *Neuroscientist*. 23:109–123.

Filmer HL, Dux PE, Mattingley JB. 2014. Applications of transcranial direct current stimulation for understanding brain function. *Trends Neurosci*. 37:742–753.

Fox MD, Corbetta M, Snyder AZ, Vincent JL, Raichle ME. 2006. Spontaneous neuronal activity distinguishes human dorsal and ventral attention systems. *Proc Natl Acad Sci*. 103:10046–10051.

Fregni F, Boggio PS, Nitsche M, Bermpohl F, Antal A, Feredoes E, Marcolin MA, Rigonatti SP, Silva MT, Paulus W. 2005. Anodal transcranial direct current stimulation of prefrontal cortex enhances working memory. *Exp Brain Res*. 166:23–30.

Fries P, Reynolds JH, Rorie AE, Desimone R. 2001. Modulation of oscillatory neuronal synchronization by selective visual attention. *Science*. 291:1560–1563.

Groß J, Kujala J, Hämäläinen M, Timmermann L, Schnitzler A, Salmelin R. 2001. Dynamic imaging of coherent sources: studying neural interactions in the human brain. *Proc Natl Acad Sci*. 98:694–699.

Handel BF, Haarmeier T, Jensen O. 2011. Alpha oscillations correlate with the successful inhibition of unattended stimuli. *J Cogn Neurosci*. 23:2494–2502.

Heinrichs-Graham E, Arpin DJ, Wilson TW. 2016. Cue-related temporal factors modulate movement-related beta oscillatory activity in the human motor circuit. *J Cogn Neurosci*. 28:1039–1051.

Heinrichs-Graham E, Kurz MJ, Gehringer JE, Wilson TW. 2017a. The functional role of post-movement beta oscillations in motor termination. *Brain Struct Funct*. 222:3075–3086.

Heinrichs-Graham E, McDermott TJ, Mills MS, Coolidge NM, Wilson TW. 2017b. Transcranial direct-current stimulation modulates offline visual oscillatory activity: a magnetoencephalography study. *Cortex*. 88:19–31.

Heinrichs-Graham E, McDermott TJ, Mills MS, Wiesman AI, Wang Y-P, Stephen JM, Calhoun VD, Wilson TW. 2018. The lifespan trajectory of neural oscillatory activity in the motor system. *Dev Cogn Neurosci*. 30:159–168.

Heinrichs-Graham E, Wilson TW. 2015a. Spatiotemporal oscillatory dynamics during the encoding and maintenance phases of a visual working memory task. *Cortex*. 69:121–130.

Heinrichs-Graham E, Wilson TW. 2015b. Coding complexity in the human motor circuit. *Hum Brain Mapp*. 36:5155–5167.

Heinrichs-Graham E, Wilson TW. 2016. Is an absolute level of cortical beta suppression required for proper movement? Magnetoencephalographic evidence from healthy aging. *NeuroImage*. 134:514–521.

Hillebrand A, Singh KD, Holliday IE, Furlong PL, Barnes GR. 2005. A new approach to neuroimaging with magnetoencephalography. *Hum Brain Mapp*. 25:199–211.

Hodes RJ, Insel TR, Landis SC. 2013. The NIH toolbox setting a standard for biomedical research. *Neurology*. 80:S1–S1.

Huang Y, Dmochowski JP, Su Y, Datta A, Rorden C, Parra LC. 2013. Automated MRI segmentation for individualized modeling of current flow in the human head. *J Neural Eng*. 10:066004.

Huang Y, Liu AA, Lafon B, Friedman D, Dayan M, Wang X, Bikson M, Doyle WK, Devinsky O, Parra LC. 2018. Correction: measurements and models of electric fields in the in vivo human brain during transcranial electric stimulation. *elife*. 7:e35178.

Hunter MA, Coffman BA, Gasparovic C, Calhoun VD, Trumbo MC, Clark VP. 2015. Baseline effects of transcranial direct current stimulation on glutamatergic neurotransmission and large-scale network connectivity. *Brain Res*. 1594:92–107.

Jang SH, Ahn SH, Byun WM, Kim CS, Lee MY, Kwon YH. 2009. The effect of transcranial direct current stimulation on the cortical activation by motor task in the human brain: an fMRI study. *Neurosci Lett*. 460:117–120.

Jasper HH. 1958. The ten-twenty electrode system of the international federation. *Electroencephalogr Clin Neurophysiol*. 10:370–375.

Jensen O, Mazaheri A. 2010. Shaping functional architecture by oscillatory alpha activity: gating by inhibition. *Front Hum Neurosci*. 4:186.

Kaller CP, Rahm B, Spreer J, Weiller C, Unterrainer JM. 2010. Dissociable contributions of left and right dorsolateral prefrontal cortex in planning. *Cereb Cortex*. 21:307–317.

Keeser D, Meindl T, Bor J, Palm U, Pogarell O, Mulert C, Brunelin J, Möller H-J, Reiser M, Padberg F. 2011. Prefrontal transcranial direct current stimulation changes connectivity of resting-state networks during fMRI. *J Neurosci*. 31:15284–15293.

Kelly SP, Lalor EC, Reilly RB, Foxe JJ. 2006. Increases in alpha oscillatory power reflect an active retinotopic mechanism for distracter suppression during sustained visuospatial attention. *J Neurophysiol*. 95:3844–3851.

Klem GH, Luders HO, Jasper HH, Elger C. 1999. The ten-twenty electrode system of the international federation. The International Federation of Clinical Neurophysiology. *Electroencephalogr Clin Neurophysiol Suppl*. 52:3–6.

Klimesch W, Sauseng P, Hanslmayr S. 2007. EEG alpha oscillations: the inhibition–timing hypothesis. *Brain Res Rev*. 53:63–88.

Kovach CK, Gander PE. 2016. The demodulated band transform. *J Neurosci Methods*. 261:135–154.

Kuo H-I, Bikson M, Datta A, Minhas P, Paulus W, Kuo M-F, Nitsche MA. 2013. Comparing cortical plasticity induced by conventional and high-definition 4×1 ring tDCS: a neurophysiological study. *Brain Stimul*. 6:644–648.

Kuo M-F, Nitsche MA. 2012. Effects of transcranial electrical stimulation on cognition. *Clin EEG Neurosci*. 43:192–199.

Lachaux JP, Rodriguez E, Martinerie J, Varela FJ. 1999. Measuring phase synchrony in brain signals. *Hum Brain Mapp*. 8:194–208.

Landau AN, Fries P. 2012. Attention samples stimuli rhythmically. *Curr Biol*. 22:1000–1004.

Lew BJ, McDermott TJ, Wiesman AI, O'neill J, Mills MS, Robertson KR, Fox HS, Swindells S, Wilson TW. 2018. Neural dynamics of selective attention deficits in HIV-associated neurocognitive disorder. *Neurology*. 91:e1860–e1869.

Liebetanz D, Nitsche MA, Tergau F, Paulus W. 2002. Pharmacological approach to the mechanisms of transcranial DC-stimulation-induced after-effects of human motor cortex excitability. *Brain*. 125:2238–2247.

Lisman JE, Jensen O. 2013. The theta-gamma neural code. *Neuron*. 77:1002–1016.

Maris E, Oostenveld R. 2007. Nonparametric statistical testing of EEG-and MEG-data. *J Neurosci Methods*. 164:177–190.

Mars RB, Grol MJ. 2007. Dorsolateral prefrontal cortex, working memory, and prospective coding for action. *J Neurosci*. 27:1801–1802.

McDermott TJ, Wiesman AI, Mills MS, Spooner RK, Coolidge NM, Proskovec AL, Heinrichs-Graham E, Wilson TW. 2019. tDCS modulates behavioral performance and the neural oscillatory dynamics serving visual selective attention. *Hum Brain Mapp*. 40:729–740.

McDonald S. 2014. Special series on the cognition battery of the NIH toolbox. *J Int Neuropsychol Soc*. 20:487–651.

Muthukumaraswamy SD, Singh KD. 2013. Visual gamma oscillations: the effects of stimulus type, visual field coverage and stimulus motion on MEG and EEG recordings. *NeuroImage*. 69:223–230.

Nitsche M, Fricke K, Henschke U, Schlitterlau A, Liebetanz D, Lang N, Henning S, Tergau F, Paulus W. 2003a. Pharmacological modulation of cortical excitability shifts induced by transcranial direct current stimulation in humans. *J Physiol*. 553:293–301.

Nitsche MA, Liebetanz D, Lang N, Antal A, Tergau F, Paulus W. 2003b. Safety criteria for transcranial direct current stimulation (tDCS) in humans. *Clin Neurophysiol*. 114:2220–2222.

Noudoost B, Moore T. 2011. Control of visual cortical signals by prefrontal dopamine. *Nature*. 474:372.

Okamoto M, Dan H, Sakamoto K, Takeo K, Shimizu K, Kohno S, Oda I, Isobe S, Suzuki T, Kohyama K. 2004. Three-dimensional probabilistic anatomical cranio-cerebral correlation via the international 10–20 system oriented for transcranial functional brain mapping. *NeuroImage*. 21:99–111.

Okamoto M, Dan I. 2005. Automated cortical projection of head-surface locations for transcranial functional brain mapping. *NeuroImage*. 26:18–28.

Paneri S, Gregoriou GG. 2017. Top-down control of visual attention by the prefrontal cortex. Functional specialization and long-range interactions. *Front Neurosci*. 11:545.

Peña-Gómez C, Sala-Lonch R, Junqué C, Clemente IC, Vidal D, Bargalló N, Falcón C, Valls-Solé J, Pascual-Leone Á, Bartrés-Faz D. 2012. Modulation of large-scale brain networks by transcranial direct current stimulation evidenced by resting-state functional MRI. *Brain Stimul*. 5:252–263.

Poreisz C, Boros K, Antal A, Paulus W. 2007. Safety aspects of transcranial direct current stimulation concerning healthy subjects and patients. *Brain Res Bull*. 72:208–214.

Proskovec AL, Heinrichs-Graham E, Wilson TW. 2016. Aging modulates the oscillatory dynamics underlying successful working memory encoding and maintenance. *Hum Brain Mapp*. 37:2348–2361.

Siegel M, Donner TH, Oostenveld R, Fries P, Engel AK. 2006. High-frequency activity in human visual cortex is modulated by visual motion strength. *Cereb Cortex*. 17:732–741.

Spaak E, de Lange FP, Jensen O. 2014. Local entrainment of alpha oscillations by visual stimuli causes cyclic modulation of perception. *J Neurosci*. 34:3536–3544.

Spooner RK, Wiesman AI, Proskovec AL, Heinrichs-Graham E, Wilson TW. 2019. Rhythmic spontaneous activity mediates the age-related decline in somatosensory function. *Cereb Cortex*. 29:680–688.

Spooner RK, Wiesman AI, Proskovec AL, Heinrichs-Graham E, Wilson TW. 2020. Prefrontal theta modulates sensorimotor gamma networks during the reorienting of attention. *Hum Brain Mapp*. 41:520–529.

Tallon-Baudry C, Bertrand O, Hénaff M-A, Isnard J, Fischer C. 2004. Attention modulates gamma-band oscillations differently in the human lateral occipital cortex and fusiform gyrus. *Cereb Cortex*. 15:654–662.

Taulu S, Simola J. 2006. Spatiotemporal signal space separation method for rejecting nearby interference in MEG measurements. *Phys Med Biol*. 51:1759.

Uusitalo MA, Ilmoniemi RJ. 1997. Signal-space projection method for separating MEG or EEG into components. *Med Biol Eng Comput*. 35:135–140.

van Asselen M, Kessels RP, Neggers SF, Kappelle LJ, Frijns CJ, Postma A. 2006. Brain areas involved in spatial working memory. *Neuropsychologia*. 44:1185–1194.

Van Dijk H, Schoffelen J-M, Oostenveld R, Jensen O. 2008. Prestimulus oscillatory activity in the alpha band predicts visual discrimination ability. *J Neurosci*. 28:1816–1823.

Van Veen BD, Van Drongelen W, Yuchtman M, Suzuki A. 1997. Localization of brain electrical activity via linearly

constrained minimum variance spatial filtering. *IEEE Trans Biomed Eng*. 44:867–880.

Vidal JR, Chaumon M, O'Regan JK, Tallon-Baudry C. 2006. Visual grouping and the focusing of attention induce gamma-band oscillations at different frequencies in human magnetoencephalogram signals. *J Cogn Neurosci*. 18:1850–1862.

Wang JX, Rogers LM, Gross EZ, Ryals AJ, Dokucu ME, Brandstatt KL, Hermiller MS, Voss JL. 2014. Targeted enhancement of cortical-hippocampal brain networks and associative memory. *Science*. 345:1054–1057.

Weber MJ, Messing SB, Rao H, Detre JA, Thompson-Schill SL. 2014. Prefrontal transcranial direct current stimulation alters activation and connectivity in cortical and subcortical reward systems: a tDCS-fMRI study. *Hum Brain Mapp*. 35:3673–3686.

Wiesman AI, Groff BR, Wilson TW. 2018a. Frontoparietal networks mediate the behavioral impact of alpha inhibition in visual cortex. *Cereb Cortex*. 29:3505–3513.

Wiesman AI, Heinrichs-Graham E, Proskovec AL, McDermott TJ, Wilson TW. 2017. Oscillations during observations: dynamic oscillatory networks serving visuospatial attention. *Hum Brain Mapp*. 38:5128–5140.

Wiesman AI, Mills MS, McDermott TJ, Spooner RK, Coolidge NM, Wilson TW. 2018b. Polarity-dependent modulation of multispectral neuronal activity by transcranial direct current stimulation. *Cortex*. 108:222–233.

Wiesman AI, O'neill J, Mills MS, Robertson KR, Fox HS, Swindells S, Wilson TW. 2018c. Aberrant occipital dynamics differentiate HIV-infected patients with and without cognitive impairment. *Brain*. 141:1678–1690.

Wiesman AI, Wilson TW. 2019. The impact of age and sex on the oscillatory dynamics of visuospatial processing. *NeuroImage*. 185:513–520.

Wiesman AI, Wilson TW. 2020. Attention modulates the gating of primary somatosensory oscillations. *NeuroImage*. 116610. https://doi.org/10.1016/j.neuroimage.2020.116610.

Wilson FA, Scalaidhe S, Goldman-Rakic PS. 1993. Dissociation of object and spatial processing domains in primate prefrontal cortex. *Science*. 260:1955–1958.

Wilson TW, Heinrichs-Graham E, Becker KM. 2014. Circadian Modulation of motor-related beta oscillatory responses. *Neuroimage*. 2:531–539.

Wilson TW, McDermott TJ, Mills MS, Coolidge NM, Heinrichs-Graham E. 2018. tDCS modulates visual gamma oscillations and basal alpha activity in occipital cortices: evidence from MEG. *Cereb Cortex*. 28:1597–1609.

Woods AJ, Antal A, Bikson M, Boggio PS, Brunoni AR, Celnik P, Cohen LG, Fregni F, Herrmann CS, Kappenman ES. 2016. A technical guide to tDCS, and related non-invasive brain stimulation tools. *Clin Neurophysiol*. 127: 1031–1048.

Worden MS, Foxe JJ, Wang N, Simpson GV. 2000. Anticipatory biasing of visuospatial attention indexed by retinotopically specific-band electroencephalography increases over occipital cortex. *J Neurosci*. 20:1–6.